CHEMISTRY & SUSTAINABILITY

CHEMSUSCHEM

ENERGY & MATERIALS

Accepted Article

Title: Metal Doping for Enhancing the Photoelectrochemical Behavior of LaFeO3 Photocathodes

Authors: María Isabel Díez-García and Roberto Gómez

To be cited as: *ChemSusChem* 10.1002/cssc.201700166

Link to VoR: http://dx.doi.org/10.1002/cssc.201700166

A Journal of

ChemPubSoc Europe

WILEY-VCH

www.chemsuschem.org

Metal Doping for Enhancing the Photoelectrochemical Behavior of $LaFeO_3$ Photocathodes

María Isabel Díez-García,[a] Roberto Gómez*[a]

Abstract: The development of tandem devices for water photosplitting requires finding photocathodic materials based on earth-abundant elements and showing long-term stability in aqueous electrolytes. Ternary metal oxides seem to be a viable option, among which perovskites stand out. In this context, transparent and compact $LaFeO_3$ thin film electrodes have been prepared by sol-gel, both undoped and doped with metals (M) such as magnesium or zinc. Pristine electrodes support the development of cathodic photocurrents in 0.1 M NaOH aqueous solutions, particularly in the presence of oxygen, with an onset potential as high as 1.4 V vs. RHE. Doping with Mg or Zn leads to an important enhancement of the photocurrent, which peaks for a stoichiometry $LaFe_{0.95}M_{0.05}O_3$ with a six-fold enhancement with respect to the pristine material. Such an improvement is attributed to an increase in both the density and mobility of the majority carriers, although a contribution of surface passivation cannot be excluded.

Introduction

Mankind is facing the challenge of changing the paradigm of energy production and storage in a sustainable way. The relevance of renewable energy production in this context is obvious. The conversion of solar energy into chemical energy has the added advantage that energy storage in the form of chemical bonds is achieved. In particular, direct water photoelectrolysis in bias-free tandem cells (containing at least one photoanode and one photocathode) is particularly attractive.[1–8] However, the development of efficient and stable photocathodes promoting water reduction is still a challenge. Many metal oxides, including those having a complex stoichiometry (i.e. ternary, quaternary oxides) behave as semiconductors and present good stability in aqueous environments, making them attractive candidates for water splitting devices. Among the ternary oxides, p-type behavior has been uncovered for some perovskites, spinels, delafossites and scheelites.[9–26] Perovskite-type oxides may be seen as a good alternative because most of them exhibit p-type semiconducting nature and high stability under illumination in aqueous solutions. For instance, $LaFeO_3$ appears as a promising candidate, and several reports investigating this material in the context of photoelectrochemistry have recently been released.[16,20,27–31] Concretely, Celorrio et al.[16] studied the properties of a nanostructured $LaFeO_3$ electrode as a photocathode, and subsequently Yu and co-workers prepared compact $LaFeO_3$ electrodes using pulsed laser deposition (PLD) and a p-$LaFeO_3$/n-Fe_2O_3 water splitting photocell stable even after 120 h.[20] It is worth noting that the development of not only cathodic, but also anodic photocurrents have been reported for this material depending on the particular conditions of the experiment. In fact, May and co-workers[29] have studied ultrathin $LaFeO_3$ films over Nb:$SrTiO_3$ prepared by PLD. For all the electrodes, anodic photocurrents are observed. In addition, cathodic photocurrents appear in the presence of O_2 for $LaFeO_3$ films with thickness equal or higher than 5 nm. Peng et al.[31] also demonstrated that nanoparticulate $LaFeO_3$ electrodes can develop either cathodic and anodic photocurrents. On the other hand, several works have focused on the properties of this material as a photoanode, reporting an enhancement of photoelectrochemical water oxidation by doping with metals[28] and by incorporating co-catalysts.[30,31] For instance, surface modification with Co-Pi as a co-catalyst leads to an increase of the n-type character, suppressing the photocathodic current and shifting the onset toward more negative values.[31]

Doping may also be an appropriate strategy for increasing the p-type character of the ternary oxides.[32] It has been reported that doping with metals having a 2+ oxidation state and radii similar to that of Fe^{3+} (such as Mg^{2+} or Zn^{2+}) triggers changes in the structural, electrical and magnetic properties of the pristine material.[33–35] Concretely, using Mg and Zn as dopants in the $LaFeO_3$ perovskite has been demonstrated to be an effective strategy for the development of gas sensors,[36–38] oxidation catalysts[34] and photocatalysts.[39]

In this work, $LaFeO_3$ thin film photoelectrodes prepared on transparent conductive substrates following a simple and scalable sol-gel procedure are shown to exhibit cathodic photocurrents in the studied range of potentials. Such a p-type character is enhanced by the partial substitution of Fe by Mg or Zn in the perovskite structure. Concretely, the photocurrent for O_2 reduction is increased up to six-fold for $LaFe_{1-x}Mg_xO_3$ and $LaFe_{1-x}Zn_xO_3$ electrodes with x=0.05. Electrochemical AC methods (Mott-Schottky and Nyquist plots) help reveal important information about the effect of the substitution of Fe by Mg and Zn on the photoresponse.

[a] M.I. Díez-García and Dr. R. Gómez
Departament de Química Física i Institut Universitari d'Electroquímica, Universitat d'Alacant, Apartat 99, E-03080 Alicante, Spain
E-mail: roberto.gomez@ua.es

Supporting information for this article is given via a link at the end of the document

Results and Discussion

Physical characterization of the electrodes

The crystalline structure of the electrodes was characterized by X-ray diffraction (XRD) using 10-layer thick electrodes in order to

improve the intensity of the diffraction peaks. Figure 1A displays the patterns of the $LaFeO_3$ together with the Mg- and Zn-doped samples for x=0.05 and 0.10. Apart from the signals associated with the FTO substrate, all the diffraction peaks in the pristine and doped samples are fully compatible with those expected for the cubic form of $LaFeO_3$ (01-075-0541 card in ICDD database), and no other phases are detected. This is in agreement with different reports that confirm the prevalence of the substitution of the Fe atoms in the perovskite structure by Mg or Zn instead of the formation of new phases, at least for dopant concentration up to x=0.3.[33,34,36,39] Field Emission Scanning Electron Microscopy (FE-SEM) images in figure 1B reveal the formation of compact films with low porosity, being the surface morphology quite similar for both pristine and doped samples.

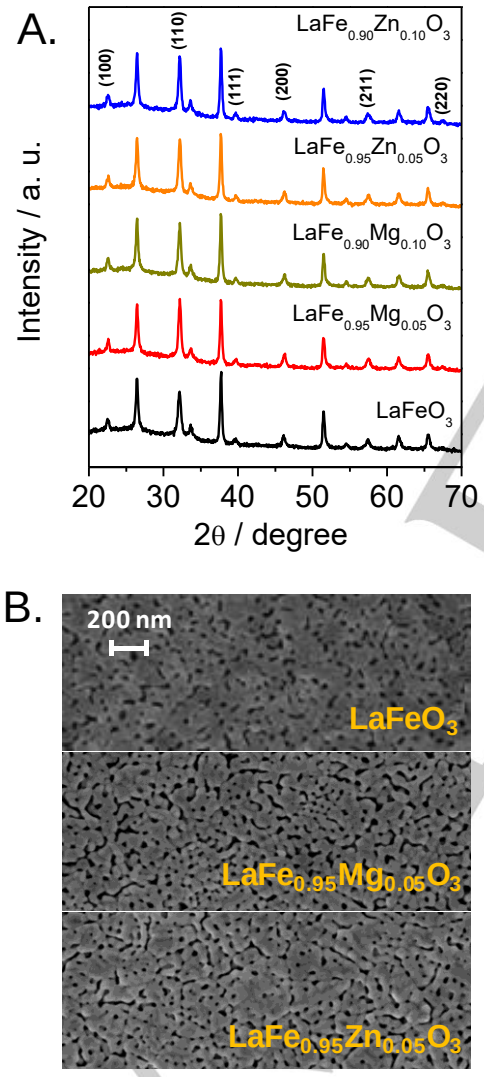

Figure 1. (A) XRD patterns and (B) FE-SEM micrographs for different pristine and doped $LaFeO_3$ electrodes.

Figure 2 shows that the high resolution XPS spectra in the La 3d, Fe 2p and O 1s regions for $LaFeO_3$ are very similar for pristine and doped samples. There are no shifts in the peak positions triggered by the introduction of Mg or Zn. In figure 2A, the La 3d doublet is located at 833.5 eV and 850.4 eV for La $3d_{5/2}$ and La $3d_{3/2}$, respectively. These peak positions[40,41] suggest the 3+ oxidation state for La, further confirmed by a spin-orbit gap of about 16.8 eV between La $3d_{5/2}$ and La $3d_{3/2}$.[42] In the Fe 2p region in figure 2B, the peak positions for Fe $2p_{3/2}$ and Fe $2p_{1/2}$ are 709.8 and 723.7 eV, respectively. The satellite at 718.0 eV is indicative of the presence of Fe^{3+}.[43] However, the binding energies are slightly lower than those reported for Fe^{3+}, and thus the presence of a minor amount of Fe^{2+} in the material cannot be discarded. The O 1s photoemission spectra (figure 2C) can be deconvoluted into three chemically shifted components in all cases. The component at the lower binding energy (528.9 eV) is assigned to oxygen in the perovskite lattice.[40] The second peak at 530.8 eV is ascribed to OH^- species, as the rare-earth oxides are highly hygroscopic. In fact, it is known that La_2O_3 absorbs water rapidly with a concomitant conversion of surface anions, giving rise to a hydroxylated surface.[40,44] Finally, the component at the highest binding energy, 532 eV, can be associated to oxygen atoms in adsorbed carbonated species rather than to adsorbed water whose signal is typically located at higher binding energy values. The carbonated species likely correspond to adventitious impurities coming from the ambient exposure of the electrode prior to the measurements.

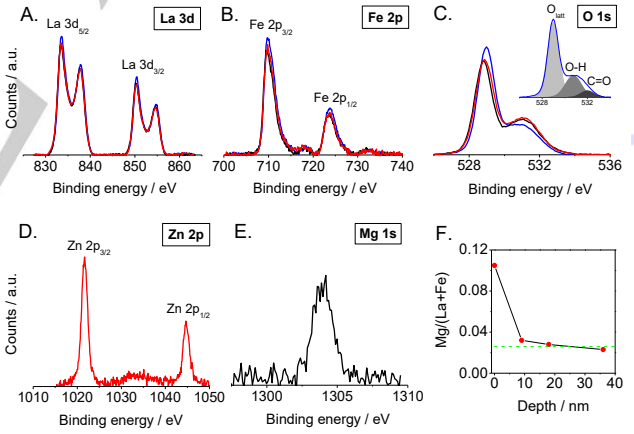

Figure 2. High resolution XPS spectra showing the (A) La 3d, (B) Fe 2p and (C) O 1s regions for the $LaFeO_3$ (blue line), $LaFe_{0.95}Mg_{0.05}O_3$ (black line) and $LaFe_{0.95}Zn_{0.05}O_3$ (red line) electrodes. The inset shows the three components resulting from the deconvolution of the O 1s spectrum for the $LaFeO_3$ sample. High resolution XPS spectra in the (D) Zn 2p region for $LaFe_{0.95}Zn_{0.05}O_3$ and (E) Mg 1s region for $LaFe_{0.95}Mg_{0.05}O_3$. (F) Atomic Mg/(La+Fe) ratio from XPS as a function of the depth for a $LaFe_{0.95}Mg_{0.05}O_3$ electrode (the green line indicates the expected value).

More importantly, X-ray photoelectron spectra (XPS) in figures 2D,E confirm the presence of either Mg or Zn at the surface. Binding energies of 1304.0 eV for Mg 1s and 1021.7 eV for Zn $2p_{3/2}$ are not surprisingly in accordance with a +2 oxidation state in both cases. More interestingly, for the $LaFe_{0.95}Mg_{0.05}O_3$ and

$LaFe_{0.95}Zn_{0.05}O_3$ electrodes, the surface ratios Mg/Fe and Zn/Fe, respectively, are 7-8 times the expected bulk concentration (table S1). The evident segregation of these ions may be correlated with the observed increase in the hydroxyl surface concentration for the doped electrodes (see table S1) due to the fact that Mg and Zn oxygenated species are more hygroscopic than Fe ones. In this respect, figure 2F shows the values of the Mg/(La+Fe) atomic ratio as a function of the depth. Magnesium segregates to the surface, although the Mg concentration is virtually constant and close to the expected value for depths equal to or greater than 9 nm.

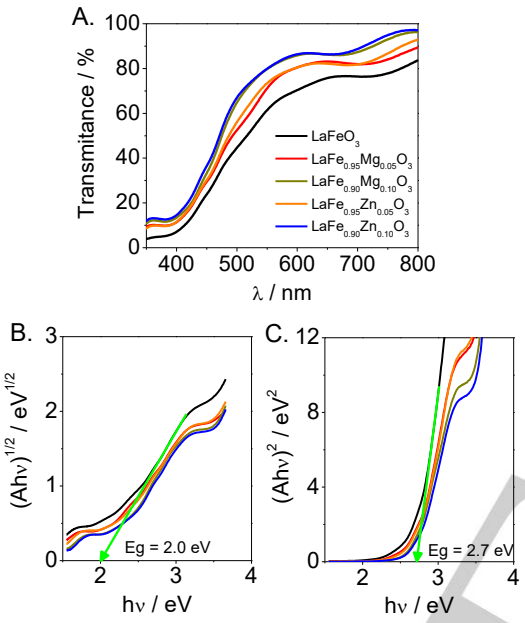

Figure 3. (A) Transmission UV-visible spectra for different pristine and doped $LaFeO_3$ electrodes and the corresponding Tauc plots for indirect (B) and direct (C) optical transitions.

Figure 3A shows the UV-vis transmittance spectra for pristine and Zn- or Mg-doped $LaFeO_3$ electrodes. The corresponding UV-visible absorbance spectrum (calculated by the KubelKa Munk function) for the pristine $LaFeO_3$ thin film electrode (figure S1) exhibits an absorption edge at about 600 nm, in agreement with an indirect optical band gap of 2.0 eV as calculated by means of a Tauc plot (figure 3B). Such a band gap value is in line with other reported values.[28,29] A direct transition band gap value of 2.7 eV can also be calculated (figure 3C), which is slightly higher than other reported values (2.47-2.56 eV) for the direct transition of $LaFeO_3$ nanoparticles,[16,27,45] and closer to the 2.65 eV value obtained for 25-55-nm thick films.[46] It is worth noting that the indirect and direct band gaps slightly change with the doping level. However, irrespective of the presence of either Mg or Zn as dopants, the transmittance vs. λ curves are virtually identical for the same value of x.

Photoelectrochemical characterization

The photoelectrochemical response for pristine and doped $LaFeO_3$ electrodes in the form of linear scan voltammograms under chopped illumination recorded in either N_2- or O_2-purged 0.1 M NaOH are shown in Figure 4. The current-potential response for the $LaFeO_3$ electrode in the N_2-purged electrolyte in Figure 4A exhibits photocathodic currents at potentials as high as 0.5 V (photocurrent onset). The photocurrent transients present spikes upon both illumination and light interruption, which indicates a high recombination rate of the charge carriers due to an effective trapping of photogenerated electrons at the surface.[47] In any case, the excellent stability of the electrodes under illumination, together with the reported ability of this material for H_2 production in photocatalysis,[48] points to the assignment of the observed photocurrent in N_2-purged electrolyte to the H_2 evolution reaction.

The presence of an electron scavenger such as O_2, induces a drastic increase in the photocurrent and a suppression of the spikes in the illumination transients at potentials lower than about 0 V, which indicates that surface electron trapping is significantly hindered in the presence of O_2. Small photocathodic currents appear at potentials as high as 0.5 V, although sizeable photocurrents only develop at potentials below 0.1 V.

Cyclic voltammograms in the dark in figure S2 reveal a capacitive region at positive potentials that fits well with the accumulation region for a p-type material.[19,24] As the potential for the onset of the photocurrent is close to the onset of the capacitive currents in the dark, such an accumulation region can tentatively be related to the filling/emptying of valence band states. In this respect, it is important to highlight that DFT calculations reveal that the upper part of the valence band mainly consists of O 2p states, with an important contribution of Fe 3d e_g states.[49,50] Then, free holes in $LaFeO_3$ can be ascribed to both O^- and Fe^{4+} species.

The above discussion reveals the p-type nature of the pristine $LaFeO_3$ perovskite, which is thought to be due to the presence of small amounts of Fe^{4+}.[51] In this respect, Porta et al.[33] have determined a Fe^{4+}/Fe_{total} ratio of 0.024 by TPR and of 0.032 by chemical titration for $LaFeO_3$ powder obtained by a sol-gel method using the citrate route. The presence of Fe^{4+} is compensated with the corresponding level of oxygen excess, yielding a stoichiometry $LaFeO_{3+\delta}$.

We analyze in the following the photoelectrochemical behavior of the doped $LaFeO_3$ electrodes. It is noteworthy that, in N_2-purged electrolyte, higher current spikes upon illumination and light interruption are developed for the doped electrodes (figure S3), although the magnitude of the stationary photocurrents remains almost unaltered. It seems thus that electron transfer from surface states to water keeps on being kinetically sluggish. In contrast with the case of the N_2-purged electrolyte, the photocurrents in the presence of O_2 dramatically increase for the doped samples.

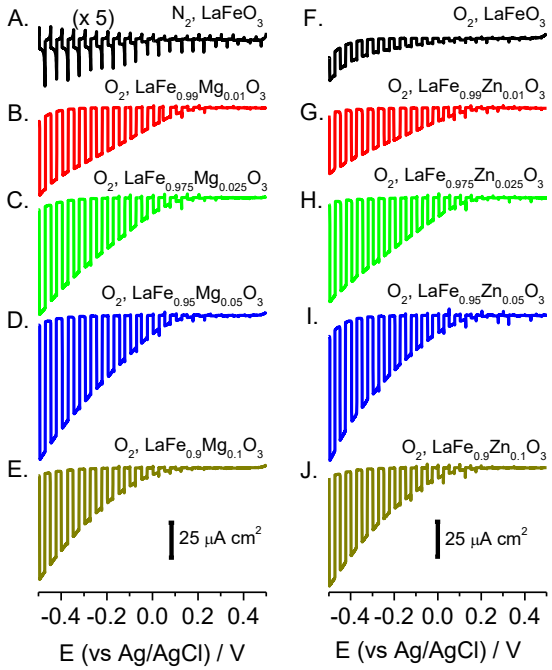

Figure 4. Linear scan voltammograms (negative-going scan) under chopped 1 sun illumination in a 0.1 M NaOH electrolyte purged with either N_2 (A) or O_2 (B-J) at a scan rate of 5 mV s^{-1} for (A) and (F) $LaFeO_3$, (B-E) $LaFe_{1-x}Mg_xO_3$ and (G-J) $LaFe_{1-x}Zn_xO_3$ electrodes with x=0.01, 0.025, 0.05 and 0.1.

Stationary currents under illumination in the presence of O_2 were also recorded for the different electrodes at -0.25 V. In figure 5A the transients for pristine $LaFeO_3$ and samples doped with x=0.05 are shown. Except for a small initial spike for the pristine material, the photocurrents are constant over the illumination time for all the electrodes, indicating again that electron surface trapping is minor. The photocurrent measured after 60 s of illumination is plotted vs. the dopant concentration in figure 5B. The stationary photocurrent increases as the dopant concentration does, reaching an optimum at x=0.05 for both dopants. Importantly, doping with equivalent quantities of either Mg or Zn leads to similar photocurrent values, which suggests that the role of Mg and Zn in the perovskite structure is similar.

For the two-layer electrode, the illumination direction (electrolyte-electrode, EE, versus substrate-electrode, SE, illumination) leads to comparable photocurrent values for both pristine and doped $LaFeO_3$ electrodes (see figure S4). This is a result of the low thinness of the electrode i) which transmits a significant fraction of the incident light and/or ii) which has a thickness smaller than the sum of the hole diffusion length and the space charge width. Electrodes containing 4 and 6 layers were also studied together with the two-layer ones (figure S5). Although the response is not dramatically dependent on the electrode thickness, the optimum photocurrent for EE illumination in the presence of O_2 is observed for the 4-layer thin film for both $LaFeO_3$ and $LaFe_{0.95}Mg_{0.05}O_3$ electrodes, reaching a value of ca. 0.1 mA·cm^{-2} for the latter.

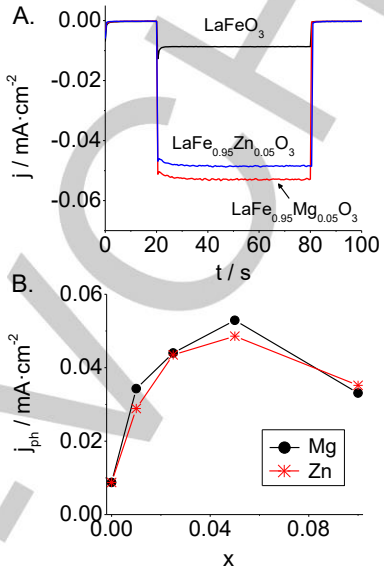

Figure 5. (A) Photocurrent transients at -0.25 V for pristine and Mg- and Zn-doped $LaFeO_3$ electrodes (x=0.05). (B) Stationary photocurrent at -0.25 V as a function of x for $LaFe_{1-x}Mg_xO_3$ and $LaFe_{1-x}Zn_xO_3$ electrodes. Electrolyte: O_2-purged 0.1 M NaOH.

To get some insights into the mechanism for photocurrent enhancement upon the introduction of Mg and Zn in the structure, the Mott-Schottky approximation was applied to investigate possible changes in carrier density and flat band potential. The C_S^{-2} vs. potential plots in figures 6A,B show a straight line of negative slope in all the cases, as expected for p-type semiconductor electrodes under band edge pinning. In addition, at potentials substantially more negative than the flat band potential, a close-to-linear region with a positive slope is observed. There are several reasons that could explain this behavior such as a contribution linked to the conducting glass substrate or a loss of the band edge pinning condition associated to a contribution of surface states.[52]

In the Mg-doped samples no shift in the flat band potential (calculated as the intercept of the straight line with the x-axis) is discernible, being located at 0.5 V. In contrast, a shift of 0.1 V toward positive potentials is observed for all the Zn-doped electrodes. The position of the valence band edge for these materials can thus be estimated to be located at 1.45-1.55 V vs. RHE, as the measured flat band potential is expected to be very close to the valence band edge location. Remarkably, the flat band potential values are located close to the observed photocurrent onset in either N_2- or O_2-purged electrolytes. If a band gap value of 2.0 eV is considered for $LaFeO_3$, the location of the VB edge would translate into a potential for the CB edge of -0.5 V vs. RHE. The band edge potentials reveal that the materials should be able to reduce both water and O_2, although

the kinetics for water photoreduction is found to be very slow. The potentials of the conduction and valence band edges would be very similar for all the studied samples, and therefore the enhancement of the photoresponse should not be ascribed to an increase in the reducing power of the photogenerated electrons. On the other hand, it is known that the slope of the straight line in the Mott-Schottky plot (figures 6A and 6B) is inversely proportional to the density of the majority charge carriers (see equation S2). Considering a dielectric constant of 75,[29,51] the calculated majority charge carrier density (N_A) for the $LaFeO_3$ electrode would be as high as $8.3 \cdot 10^{18}$ cm^{-3}. A generalized drop in the slope values is observed as the dopant concentration increases (table S2), which can be attributed to an increase in hole density. This effect is especially notable for the highest concentrations of Mg and Zn, while a minor change (if any) is observed for the lowest x values. As a caveat, the quantitative information obtained from the Mott-Schottky analysis should be taken with caution given the rather stringent conditions that need to be met for its full validity. The existence of frequency dispersion coming from frequency–dependent values of the dielectric constant and/or the contribution of surface states, or the fact that the electrode surface is rough may give significant errors in the values of the flat band potential and N_A.[52,53]

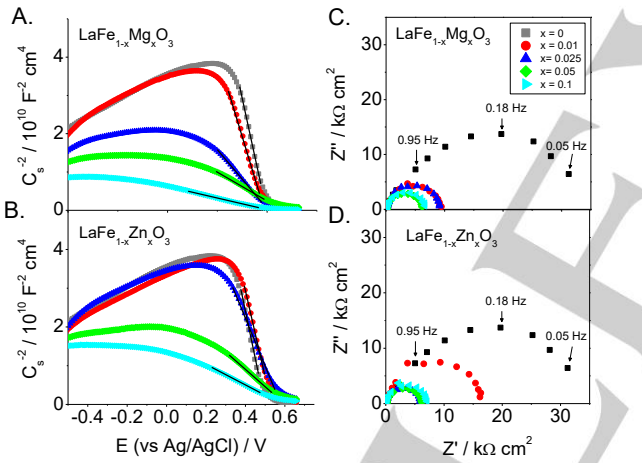

Figure 6. (A) and (B) Mott-Schottky plots in the dark at a frequency of 1 kHz for pristine and doped $LaFeO_3$ electrodes in N_2-purged 0.1 M NaOH electrolyte; (C) and (D) Nyquist plots under illumination at -0.25 V in O_2-purged 0.1 M NaOH electrolyte for pristine and doped $LaFeO_3$ electrodes.

Nyquist plots under illumination at -0.25 V in the presence of O_2 are shown in Figure 6C,D for the different electrodes studied. One semicircle is observed in all the cases. A generalized decrease in the impedance values (semicircle radius) is noticeable with the increment of Zn and Mg content. The decrease in impedance is correlated with the increment in stationary photocurrent with x in figure 5B and it can also be associated with a higher photogenerated electron flow toward the surface as advanced in models developed for understanding the EIS response of photoelectrodes.[25,54] Peng et al.[28] also observed lower impedance values for $LaFeO_3$ electrode after doping with Mn, Co and Cu, which they related to a decrease in either charge transport or charge transfer resistance.

It is noteworthy that an increase of conductivity with the introduction of Zn in $LaFeO_3$ has been reported.[35] The resistivity has also been shown to decrease with increasing values of x for $LaFe_{1-x}Mg_xO_3$ and $LaFe_{1-x}Zn_xO_3$ in gas sensing applications.[36,38] In addition, studies about the doping effect in other semiconductor oxide materials have led to the same conclusion for doping levels similar to those employed in the present work.[55,56] From the experiments discussed above, one may also conclude that an increase in bulk electrical conductivity is induced by the introduction of Mg and Zn in the perovskite structure. Electrical conductivity (σ) depends on the density (N_A) and mobility (μ) of the majority carries, as $\sigma = N_A \bullet \mu \bullet e$, where e is the elementary charge. The contribution of N_A in the conductivity enhancement is evident, as deduced from the Mott-Schottky plots. Although precise values of N_A cannot be calculated (the dielectric constant is expected to change with the dopant concentration), an increase in the charge carrier density of around one order of magnitude for x=0.1 with respect to pristine $LaFeO_3$ may be estimated. This is in accordance with the increase of the Fe^{4+}/Fe_{total} ratio upon Mg doping observed by Porta et al.[33] for $LaFe_{1-x}Mg_xO_{3+\delta}$. When the trivalent Fe ions are substituted by the divalent ions Mg or Zn, charge compensation may be accomplished either by the oxidation of Fe^{3+} to Fe^{4+} or by a partial loss of the oxygen excess (that is, by decreasing δ). The unusual small change in the majority carrier density for the lowest x values (despite the Mg or Zn content is relatively high) may be due to a loss of excess oxygen almost tantamount to the density of divalent cations introduced, rather than to an increase in Fe^{4+} density. This observation could also be related to a significant surface segregation of the dopant, as revealed by XPS (see discussion above), which would lead to a lower level of material bulk modification. However, the fact that the dopant enrichment is limited to the surface implies that this is not a main factor.

On the basis of the previous discussion, the enhancement of the photoelectrochemical response upon doping cannot be explained solely on the basis of an increase in N_A. It seems thus that there also exists a contribution coming from a higher hole mobility. The increase of μ with dopant concentration has been reported for In_2O_3 with several metal dopants (such as W, Mo, and Ti),[55–57] and also for the perovskite $SrTiO_3$ doped with La,[58] and it has been linked to lattice distortion triggered by doping. In fact, several reports have pointed out a variation of the unit cell parameters of the $LaFeO_3$ perovskite structure with the introduction of Zn and Mg divalent ions.[33,35,36,38,39] This variation has been associated to a combined effect of the larger substituting Zn^{2+} (74.5 pm) or Mg^{2+} (72.0 pm) ions in the octahedral B-site in comparison with Fe^{3+} (64.5 pm) and to the oxidation of Fe^{3+} to the smaller Fe^{4+} (58.5 pm).

It is important to mention that a surface passivation effect in the doped samples cannot be discarded. It would be caused by the segregation of Mg and Zn to the surface and its subsequent further hydroxylation, confirmed by XPS (figure 2). The decrease in the semicircle radii with the doping level could also be linked to an enhancement of the electron transfer at the interface (a

decrease in the charge transfer resistant) caused by the Mg- and Zn-induced passivation of surface recombination centers, as previously discussed. However, the fact that the photocurrents for water photoreduction remain almost unaltered upon doping suggests that this effect is minor.

Conclusions

In summary, sol-gel synthesized perovskite $LaFeO_3$ electrodes can be used as stable photocathodes for oxygen (and water) reduction. Their efficiency as photocathodes for oxygen reduction can be drastically improved by doping with relatively large amounts of Mg^{2+} and Zn^{2+} (5% with respect to iron atoms). This effect is primarily attributed to an increase in majority carrier concentration resulting from a dopant-induced increase of the Fe^{4+} density caused by charge compensation upon substitution of Fe^{3+} by Mg^{2+} and Zn^{2+}. In addition, the distortions induced by the introduction of the dopants likely increase hole mobility. In addition, a contribution coming from Zn- or Mg-induced passivation cannot be excluded as XPS points to their accumulation in the surface of the material. In principle, these electrodes have the potential to be applied as photocathodes in tandem devices because of their very positive onset potential values and their relatively narrow band gap. In addition, $LaFeO_3$ is an attractive candidate because of its stability, environmental friendliness and the relatively high earth abundance of the constituent elements. Admittedly, the kinetics of the transfer of photogenerated electrons to water needs to be enhanced as they tend to get trapped at surface states thus favoring recombination. Several strategies can be followed with this aim, including the use of appropriate co-catalysts and/or passivating layers. Experiments along these lines are underway in our laboratory.

Experimental Section

Thin film preparation

A citric sol-gel route is employed for the preparation of the different films using FTO conducting glass as a substrate. To synthesize the pristine $LaFeO_3$ sample, $La(NO_3)_3{\cdot}6H_2O$ (0.3 M) and $Fe(NO_3)_3{\cdot}9H_2O$ (0.3 M) were dissolved in water and the solution was stirred for 1 h. Then, the appropriate amount of citric acid monohydrate was added to reach a concentration of 0.6 M and the solution was stirred again for 20 h. The $LaFe_{1-x}Mg_xO_3$ and $LaFe_{1-x}Zn_xO_3$ (with x=0.01, 0.025, 0.05 and 0.1) electrodes were obtained using the above described procedure, but substituting the corresponding amount of the Fe salt by $Mg(NO_3)_2{\cdot}6H_2O$ or $Zn(NO_3)_2{\cdot}6H_2O$ according to the final desired stoichiometry.

The above mentioned solutions were mixed with acetylacetone (30 μL/mL) and Triton 100X (30 μL/mL) and the resultant liquid was spin-coated on an FTO substrate at a rotating speed of 3000 rpm for 20 s and then the samples were calcined at 500 °C for 1 h. This procedure was repeated twice (2-layers) and a final heat treatment at 640 °C for 2 h was applied, in order to obtain the crystalline perovskite films. The thickness of the resulting electrodes was 80-100 nm (two-layer electrodes), as measured with an Alpha Step D-100 profilometer. Thicker electrodes can be obtained by increasing the number of spin-coating and calcination cycles. Unless otherwise stated, the results are referred to two-layer electrodes.

Physical and chemical characterization.

A morphological examination of the films was carried out by Field Emission Scanning Electron Microscopy (FE-SEM) with a JEOL JEM-1400 microscope. The crystal structure was studied by X-ray diffraction (XRD) with a Seifert JSO-Debyeflex 2002 diffractometer using the Cu Kα line (λ= 1.5406 Å). The optical characterization of the 10-layer thick $LaFeO_3$, $LaFe_{1-x}Mg_xO_3$ and $LaFe_{1-x}Zn_xO_3$ electrodes (with x=0.05 and 0.1) was performed by measuring their UV-visible transmittance spectra using an FTO piece as a blank by means of a Shimadzu UV-2401PC spectrophotometer. Core level photoemission spectra were collected in normal emission at room temperature with a (K-Alpha of Thermo-Scientific) X-ray Photoelectron Spectrometer (XPS) using an Al Kα X-ray source and equipped with an Ar ion sputter gun to perform depth profile analysis. Ta_2O_5 was used as a reference to estimate the depth.

Photoelectrochemical experiments.

(Photo)electrochemical measurements were performed at room temperature in a three-electrode cell equipped with a fused silica window. All the potentials were measured against and are referred to an Ag/AgCl/KCl (3 M) reference electrode. A platinum wire was used as a counter electrode and an either N_2 or O_2-purged 0.1 M NaOH (Panreac, p.a.) solution as a working electrolyte. The photoelectrochemical experiments were controlled by an Autolab PGSTAT30 potentiostat coupled with a frequency response analyzer. All the impedance measurements were performed using a 10 mV amplitude perturbation. Mott-Schottky plots were performed at 1 kHz and using a potential step of 10 mV. Experiments at constant potential were measured in a frequency range from 50 mHz to 10 kHz. The electrodes were irradiated with 1 sun (100 mW cm^{-2}) illumination from the electrolyte-electrode side (EE illumination) using a solar simulator SUN 2000 (Abet Technologies).

Acknowledgements

Financial support from the Spanish Ministry of Economy and Competitiveness through project MAT2015-71727-R (FONDOS FEDER) is gratefully acknowledged.

Keywords: $LaFeO_3$ • p-type perovskite • photocathode • Mg and Zn doping • water photosplitting

[1] M. Gratzel, *Nature* **2001**, *414*, 338–344.
[2] M. G. Walter, E. L. Warren, J. R. McKone, S. W. Boettcher, Q. Mi, E. A. Santori, N. S. Lewis, *Chem. Rev*. **2010**, *110*, 6446–6473.
[3] F. E. Osterloh, B. A. Parkinson, *MRS Bull.* **2011**, *36*, 17–22.
[4] B. A. Pinaud, J. D. Benck, L. C. Seitz, A. J. Forman, Z. Chen, T. G. Deutsch, B. D. James, K. N. Baum, G. N. Baum, S. Ardo, H. Wang, E. Miller, T. F. Jaramillo, *Energy Environ. Sci.* **2013**, *6*, 1983–2002.
[5] K. Sivula, M. S. Prevot, *J. Phys. Chem. C* **2013**, *117*, 17879–17893.
[6] F. E. Osterloh, *Chem. Soc. Rev.* **2013**, *42*, 2294–320.
[7] L. M. Peter, *Electroanalysis* **2015**, *27*, 864–871.
[8] K. Zhang, M. Ma, P. Li, D. H. Wang, J. H. Park, *Adv. Energy Mater.* **2016**, *6*, 1600602.

[9] Y. Matsumoto, M. Omae, K. Sugiyama, E. Sato, *J. Phys. Chem.* **1987**, *91*, 577–581.
[10] S. Ida, K. Yamada, T. Matsunaga, H. Hagiwara, Y. Matsumoto, T. Ishihara, *J. Am. Chem. Soc.* **2010**, *132*, 17343–17345.
[11] U. A. Joshi, A. M. Palasyuk, P. A. Maggard, *J. Phys. Chem. C* **2011**, *115*, 13534–13539.
[12] K. Iwashina, A. Kudo, *J. Am. Chem. Soc.* **2011**, *133*, 13272–13275.
[13] J. Cao, T. Kako, P. Li, S. Ouyang, J. Ye, *Electrochem. Commun.* **2011**, *13*, 275–278.
[14] C. G. Read, Y. Park, K.-S. Choi, *J. Phys. Chem. Lett.* **2012**, *3*, 1872–1876.
[15] N. T. Hahn, V. C. Holmberg, B. A. Korgel, C. B. Mullins, *J. Phys. Chem. C* **2012**, *116*, 6459–6466.
[16] V. Celorrio, K. Bradley, O. J. Weber, S. R. Hall, D. J. Fermín, *ChemElectroChem* **2014**, *1*, 1667–1671.
[17] J. Gu, Y. Yan, J. W. Krizan, Q. D. Gibson, Z. M. Detweiler, R. J. Cava, A. B. Bocarsly, *J. Am. Chem. Soc.* **2014**, *136*, 830–833.
[18] M. S. Prévot, N. Guijarro, K. Sivula, *ChemSusChem* **2015**, *8*, 1359–1367.
[19] A. K. Díaz-García, T. Lana-Villarreal, R. Gómez, *J. Mater. Chem. A* **2015**, *3*, 19683–19687.
[20] Q. Yu, X. Meng, T. Wang, P. Li, L. Liu, K. Chang, G. Liu, J. Ye, *Chem. Commun.* **2015**, *51*, 3630–3633.
[21] S. Kamimura, M. Higashi, R. Abe, T. Ohno, *J. Mater. Chem. A* **2016**, *4*, 6116–6123.
[22] S. P. Berglund, F. F. Abdi, P. Bogdanoff, A. Chemseddine, D. Friedrich, R. van de Krol, *Chem. Mater.* **2016**, *28*, 4231–4242.
[23] D. Kang, J. C. Hill, Y. Park, K.-S. Choi, *Chem. Mater.* **2016**, *28*, 4331–4340.
[24] M. I. Díez-García, T. Lana–Villarreal, R. Gómez, *ChemSusChem* **2016**, *9*, 1504–1512.
[25] M. I. Díez-García, R. Gómez, *ACS Appl. Mater. Interfaces* **2016**, *8*, 21387–21397.
[26] L. Wang, H. Tang, Y. Tian, *J. Power Sources* **2016**, *319*, 210–218.
[27] I. N. Sora, F. Fontana, R. Passalacqua, C. Ampelli, S. Perathoner, G. Centi, F. Parrino, L. Palmisano, *Electrochim. Acta* **2013**, *109*, 710–715.
[28] Q. Peng, B. Shan, Y. Wen, R. Chen, *Int. J. Hydrogen Energy* **2015**, *40*, 15423–15431.
[29] K. J. May, D. P. Fenning, T. Ming, W. T. Hong, D. Lee, K. A. Stoerzinger, M. D. Biegalski, A. M. Kolpak, Y. Shao-Horn, *J. Phys. Chem. Lett.* **2015**, *6*, 977–985.
[30] Q. Peng, Y. Wen, B. Shan, R. Chen, *ECS Trans*. **2015**, *64*, 27–35.
[31] Q. Peng, J. Wang, Y. W. Wen, B. Shan, R. Chen, *RSC Adv.* **2016**, *6*, 26192–26198.
[32] J. D. Perkins, T. R. Paudel, A. Zakutayev, P. F. Ndione, P. A. Parilla, D. L. Young, S. Lany, D. S. Ginley, A. Zunger, N. H. Perry, Y. Tang, M. Grayson, T. O. Mason, J. S. Bettinger, Y. Shi, M. F. Toney, *Phys. Rev. B* **2011**, *84*, 205207.
[33] P. Porta, S. Cimino, S. De Rossi, M. Faticanti, G. Minelli, I. Pettiti, *Mater. Chem. Phys.* **2001**, *71*, 165–173.
[34] P. Ciambelli, S. Cimino, S. De Rossi, L. Lisi, G. Minelli, P. Porta, G. Russo, *Appl. Catal. B Environ.* **2001**, *29*, 239–250.
[35] I. Bhat, S. Husain, W. Khan, S. I. Patil, *Mater. Res. Bull.* **2013**, *48*, 4506–4512.
[36] S. Huang, H. Qin, P. Song, X. Liu, L. Li, R. Zhang, J. Hu, H. Yan, M. Jiang, *J. Mater. Sci.* **2007**, *42*, 9973–9977.
[37] X. Liu, B. Cheng, J. Hu, H. Qin, M. Jiang, *Sensors Actuators B Chem.* **2008**, *133*, 340–344.
[38] X. Liu, B. Cheng, J. Hu, H. Qin, M. Jiang, *Sensors Actuators B Chem*. **2008**, *129*, 53–58.
[39] S. Dong, K. Xu, G. Tian, *J. Mater. Sci.* **2009**, *44*, 2548–2552.
[40] S. Mickevičius, S. Grebinskij, V. Bondarenka, B. Vengalis, K. Šliužiene, B. A. Orlowski, V. Osinniy, W. Drube, *J. Alloys Compd.* **2006**, *423*, 107–111.
[41] Y.-G. Cho, K.-H. Choi, Y.-R. Kim, J.-S. Jung, S.-H. Lee, *Bull. Korean Chem. Soc* **2009**, *30*, 1368–1372.
[42] Z. Dai, C. Lee, B. Kim, C.-H. Kwak, J.-W. Yoon, H.-M. Jeong, J.-H. Lee, *ACS Appl. Mater. Interfaces* **2014**, *6*, 16217-16226.
[43] T. Yamashita, P. Hayes, *Appl. Surf. Sci.* **2008**, *254*, 2441–2449.
[44] A. M. De Asha, J. T. S. Critchley, R. M. Nix, *Surf. Sci.* **1998**, *405*, 201–214.
[45] L. Li, X. Wang, Y. Zhang, *Mater. Res. Bull.* **2014**, *50*, 18–22.
[46] M. D. Scafetta, Y. J. Xie, M. Torres, J. E. Spanier, S. J. May, *Appl. Phys. Lett.* **2013**, 102, 081904.
[47] P. Salvador, *J. Phys. Chem.* **1985**, *89*, 3863–3869.
[48] S. N. Tijare, M. V. Joshi, P. S. Padole, P. A. Mangrulkar, S. S. Rayalu, N. K. Labhsetwar, *Int. J. Hydrogen Energy* **2012**, *37*, 10451–10456.
[49] Z. Yang, Z. Huang, L. Ye, X. Xie, *Phys. Rev. B* **1999**, *60*, 15674–15682.
[50] J. E. Kleibeuker, Z. Zhong, H. Nishikawa, J. Gabel, A. Müller, F. Pfaff, M. Sing, K. Held, R. Claessen, G. Koster, G. Rijnders, *Phys. Rev. Lett.* **2014**, *113*, 237402.
[51] M. Idrees, M. Nadeem, M. Atif, M. Siddique, M. Mehmood, M. M. Hassan, *Acta Mater.* **2011**, *59*, 1338–1345.
[52] F. Cardon, W. P. Gomes, *J. Phys. D: Appl. Phys.* **1978**, *11*, L63-L67.
[53] A. Cots, D. Cibrev, P. Bonete, R. Gómez, *ChemElectroChem*, **2017**, doi: 10.1002/celc.201600644.
[54] W. H. Leng, Z. Zhang, J. Q. Zhang, C. N. Cao, *J. Phys. Chem. B* **2005**, *109*, 15008–15023.
[55] P. F. Newhouse, C.-H. Park, A. Keszler, J. Tate, P. S. Nyholm, *Appl. Phys. Lett.* **2005**, *87*, 112108.
[56] N. Yamada, T. Tatejima, H. Ishizaki, T. Nakada, *Jpn. J. Appl. Phys.* **2006**, *45*, L1179–L1182.
[57] Y. Abe, N. Ishiyama, *J. Mater. Sci.* **2006**, *41*, 7580–7584.
[58] T. Okuda, K. Nakanishi, S. Miyasaka, Y. Tokura, *Phys. Rev. B* **2001**, *63*, 113104.

FULL PAPER

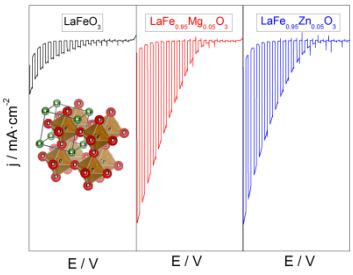

Doping is the answer. Mg- and Zn-doping of $LaFeO_3$ constitutes a step forward toward stable and efficient earth-abundant metal oxide photocathodes for artificial photosynthesis. A significant multiplication of the photocurrent is observed, particularly for oxygen reduction, without paying the price of low stability.

*María I. Díez-García, Roberto Gómez**

Page No. – Page No.

Metal Doping for Enhancing the Photoelectrochemical Behavior of $LaFeO_3$ Photocathodes